Supplementary Information

"The local cooling potential of land restoration in Africa"

Jessica Ruijsch, Adriaan J. Teuling, Gregory Duveiller, Ronald W.A. Hutjes

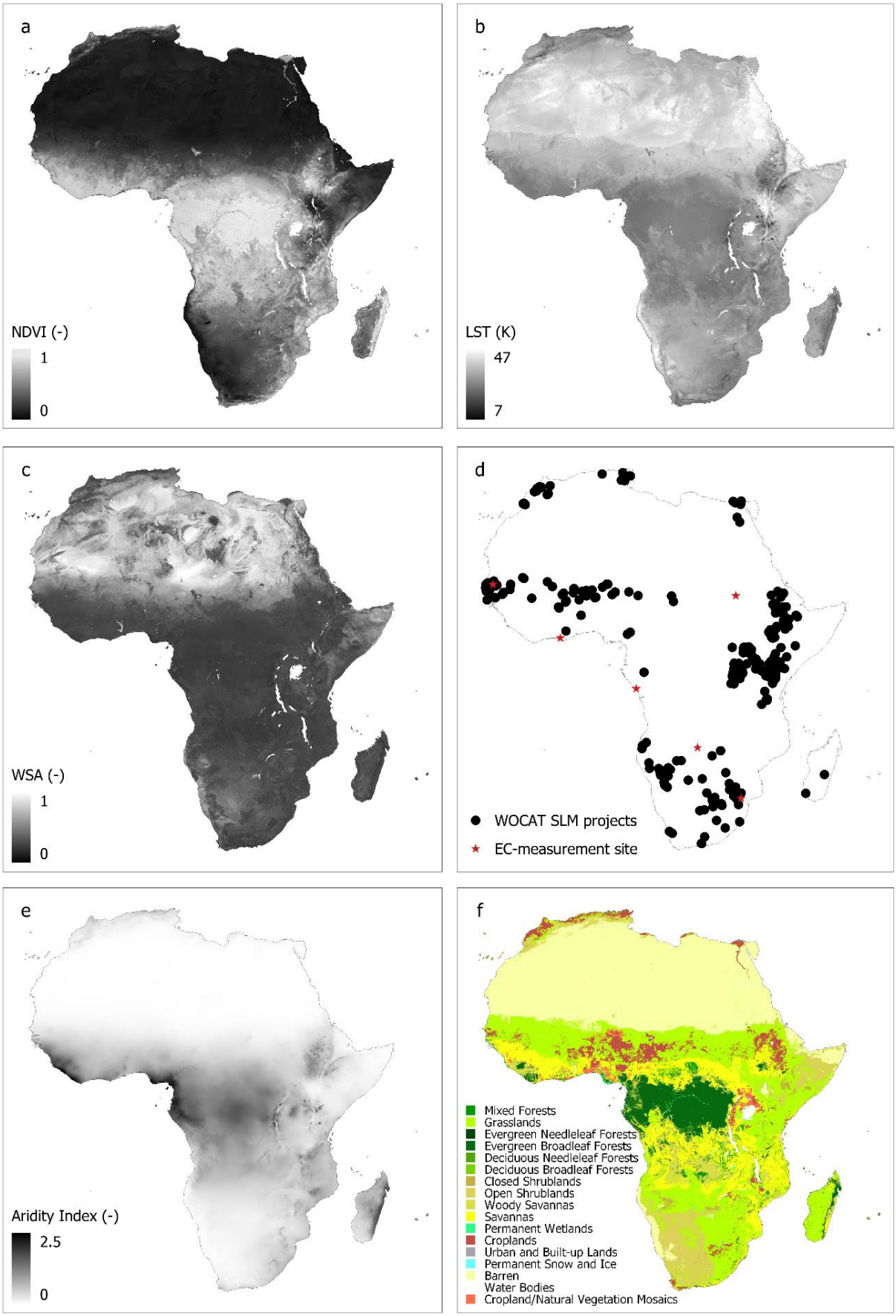

Supplementary Fig. 1 | Input data. Median Normalized Difference Vegetation Index (NDVI) (**a**), land surface temperature (LST) (**b**) and white-sky albedo (**c**) over the study period. Location of WOCAT sustainable land management projects and Eddy-covariance (EC) flux tower sites (**d**). Aridity index and over 1970-2000 (**e**). Land cover in 2001 (**f**).

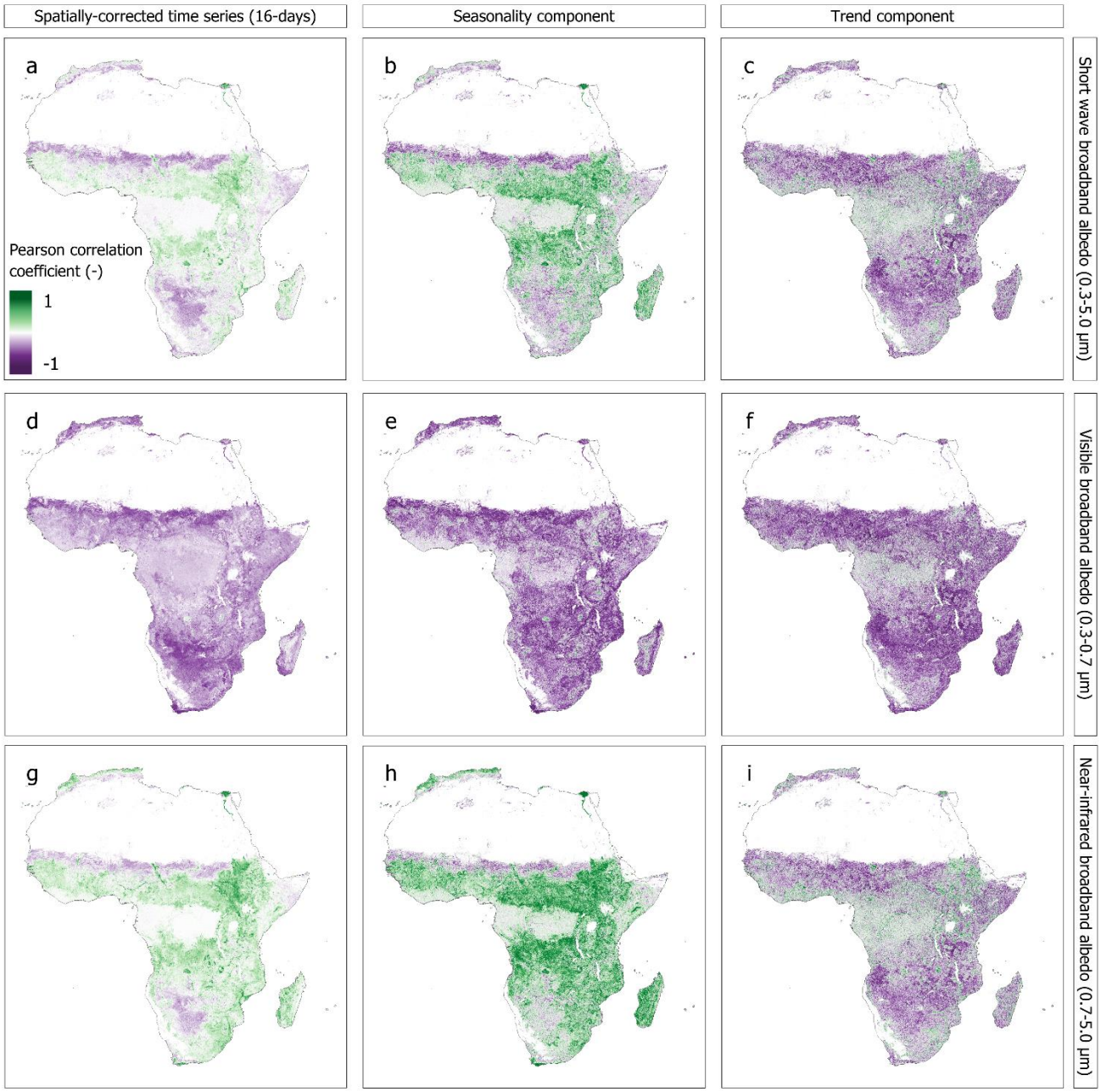

Supplementary Fig. 2 | Effect of albedo range on NDVI-WSA correlation. The pearson correlation coefficient between the NDVI and WSA for the shortwave broadband albedo (0.3-5.0 µm) (**a-c**), the visible broadband albedo (0.3-0.7 µm) (**d-f**) and the near-infrared broadband albedo (0.7-5.0 µm) (**g-i**) of the 16-day, seasonal and trend components.

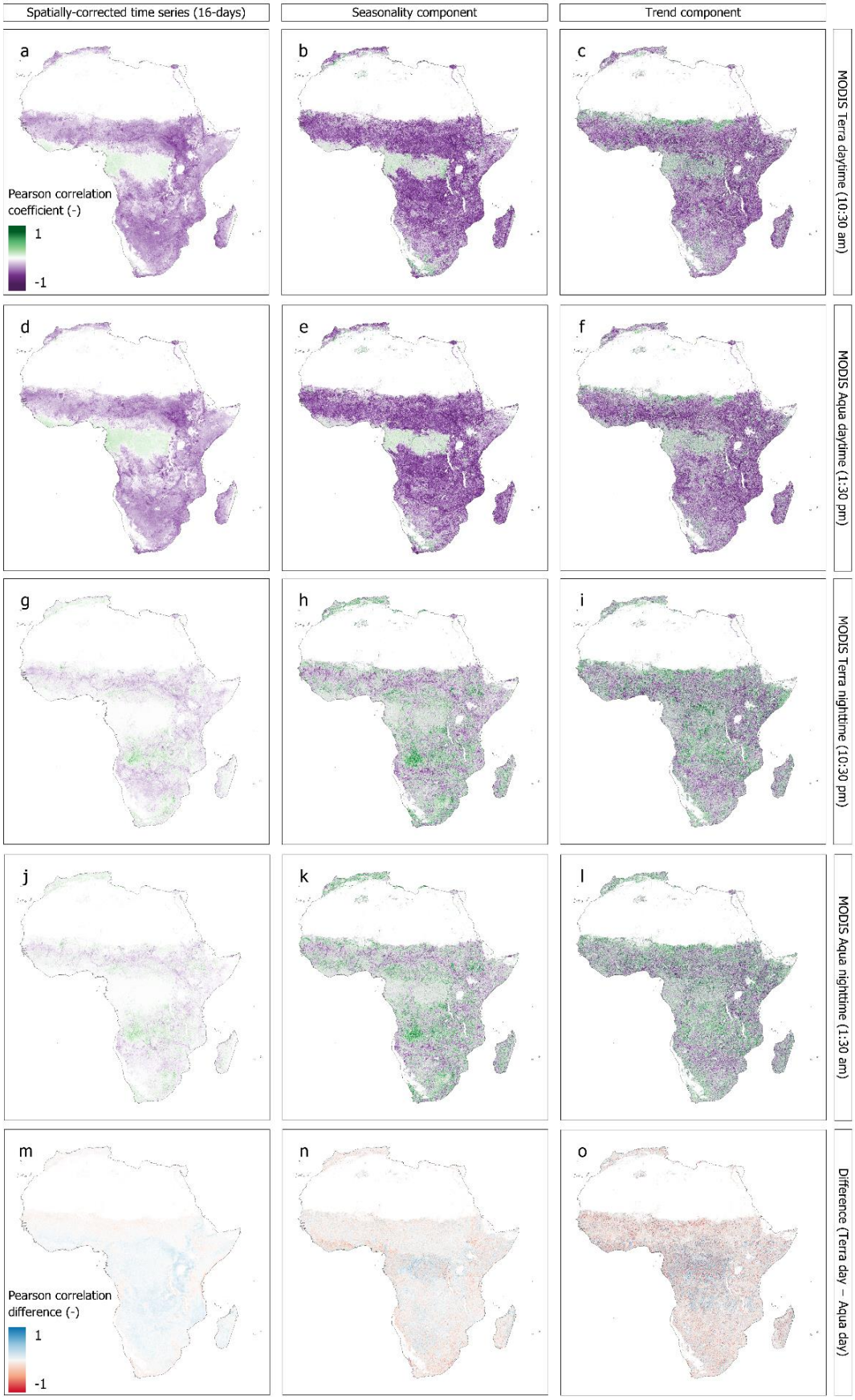

Supplementary Fig. 3 |Effect of overpass time and algorithm on NDVI-LST correlation. The 16-day pearson correlation coefficient between NDVI and LST for MODIS Terra day-time LST (overpass 10:30) (**a-c**), Aqua day-time LST (overpass 13:30) (**d-f**), Terra night-time (overpass 22:30) (**g-i**) and Aqua night-time LST (overpass 01:30) (**j-l**) of the 16-day, seasonal and trend components. (**m-o**) Difference in pearson correlation between MODIS Terra day-time and MODIS Aqua day-time.

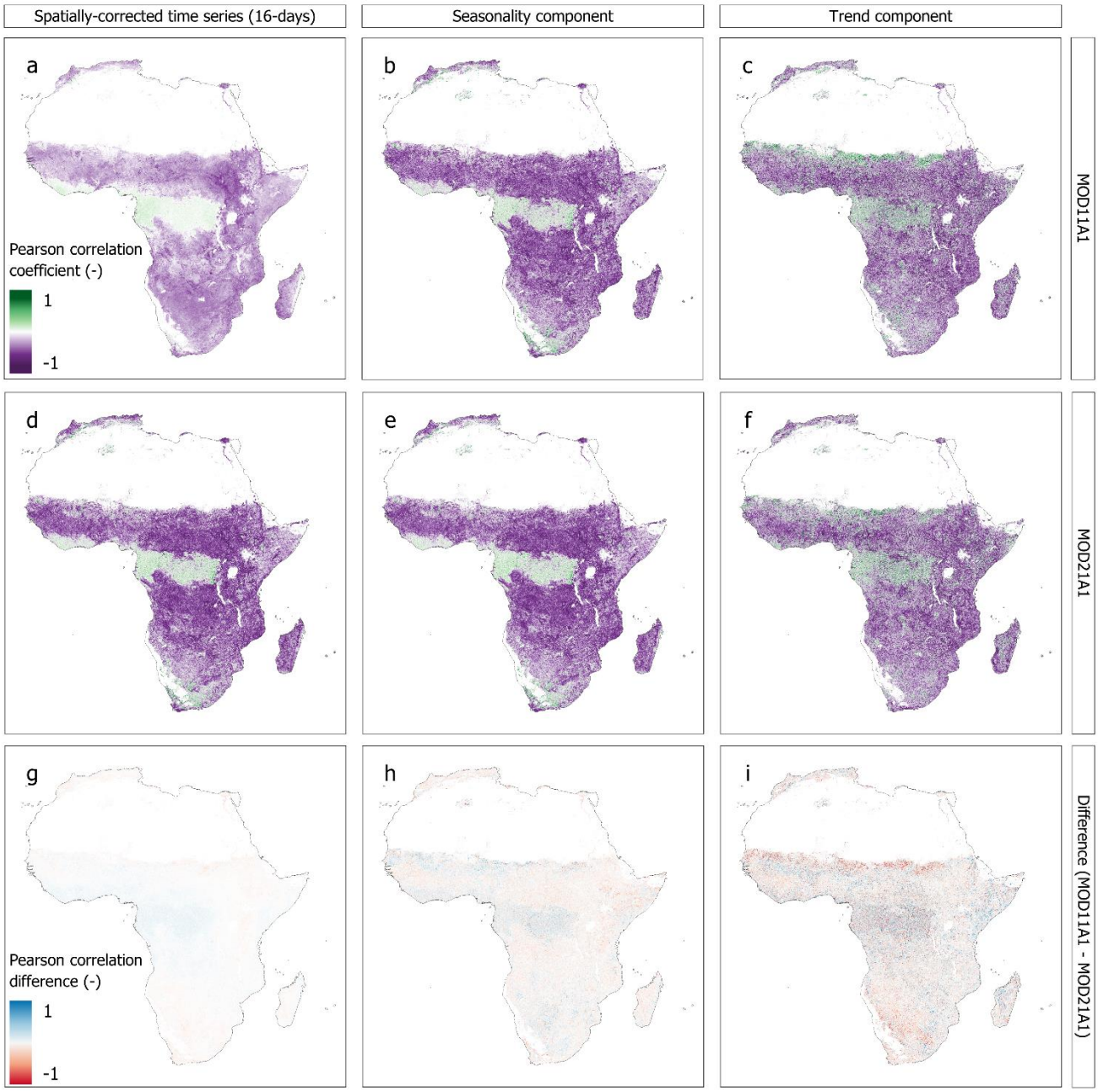

Supplementary Fig. 4 | Effect of LST algorithm on NDVI-LST correlations. The pearson correlation coefficient between the NDVI and LST for the MOD11A1 dataset (**a-c**) and the MOD21A1 dataset (**d-f**) of the 16-day, seasonal and trend components. (**g-i**) show the difference in pearson correlation coefficient between the MOD11A1 dataset and the MOD21A dataset.

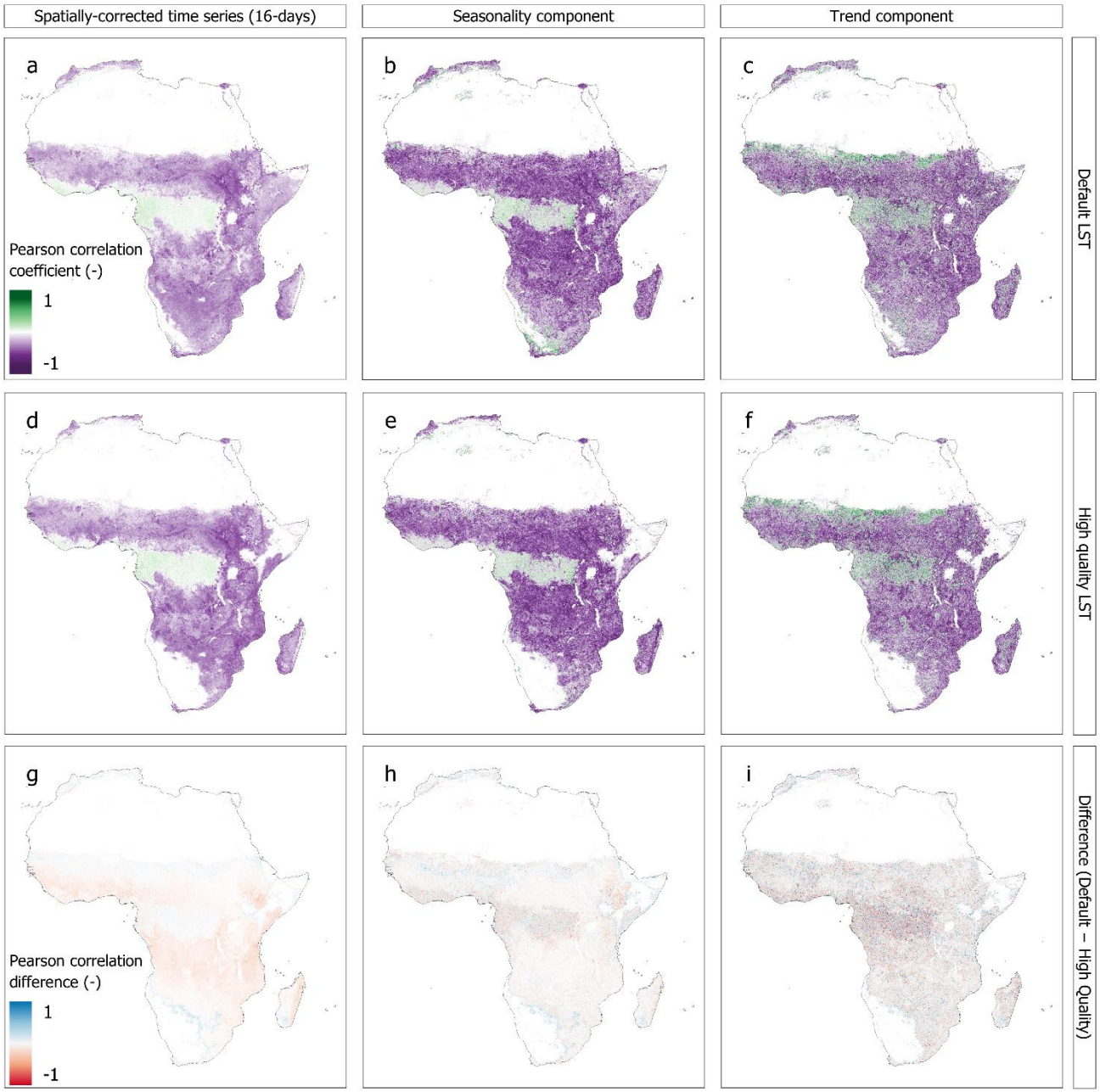

Supplementary Fig. 5 | Effect of LST quality selection on NDVI-LST correlations. The pearson correlation coefficient between the NDVI and LST for the uncorrected (**a-c**) and the quality corrected (**d-f**) of the 16-day, seasonal and trend components. (**g-i**) show the difference in pearson correlation coefficient between the uncorrected dataset and the corrected dataset.

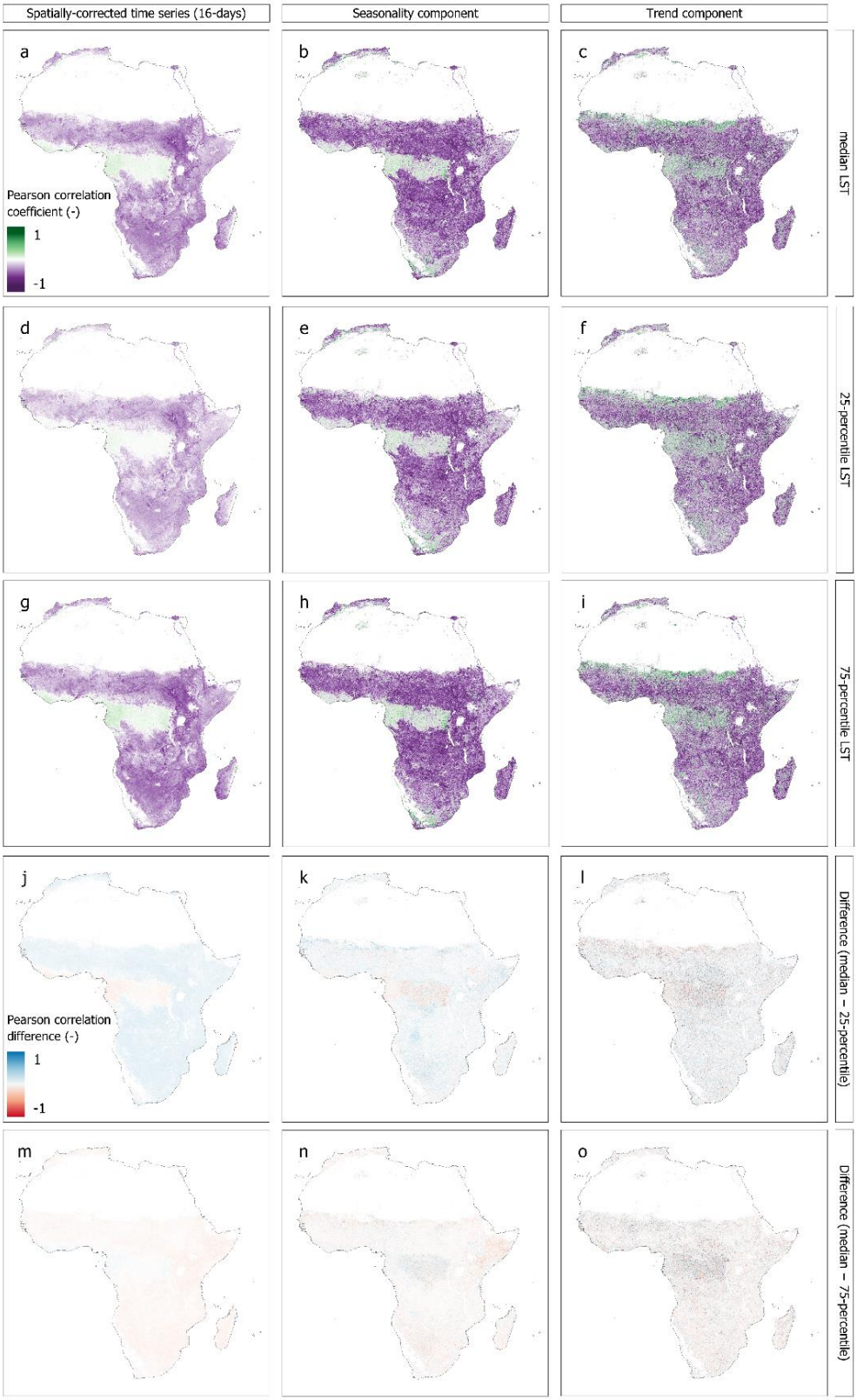

Supplementary Fig. 6 | Effect of LST temporal downscaling on NDVI-LST correlations. The LST is downscaled to a 16-day period by taking the median value of this 16-day period. This figure shows the sensitivity of the NDVI-LST correlations to the downscaling method with: the pearson correlation coefficient between the NDVI and median LST (**a-c**), 25-percentile LST (**d-f**) and 75-percentile LST (**g-i**) of the 16-day, seasonal and trend components. (**j-l**) show the difference in pearson correlation coefficient between the median LST dataset and the 25-percentile dataset. (**m-o**) show the difference in pearson correlation coefficient between the median LST dataset and the 75-percentile dataset.

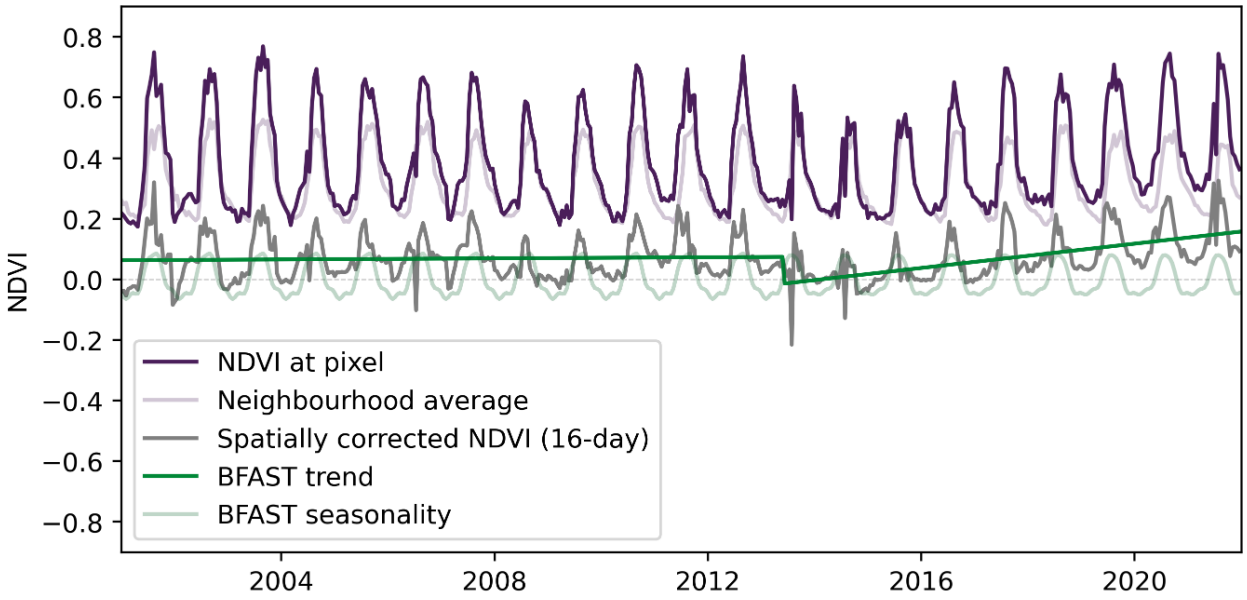

Supplementary Fig. 7 | Visualization of spatial context method and BFAST algorithm. NDVI time series at pixel, time series averaged over a neighbourhood around the centre pixel and the spatially corrected time series (i.e. the difference between the pixel and neighbourhood NDVI). The BFAST algorithm is applied to the spatially corrected 16-day time series, resulting in a seasonality and trend component.

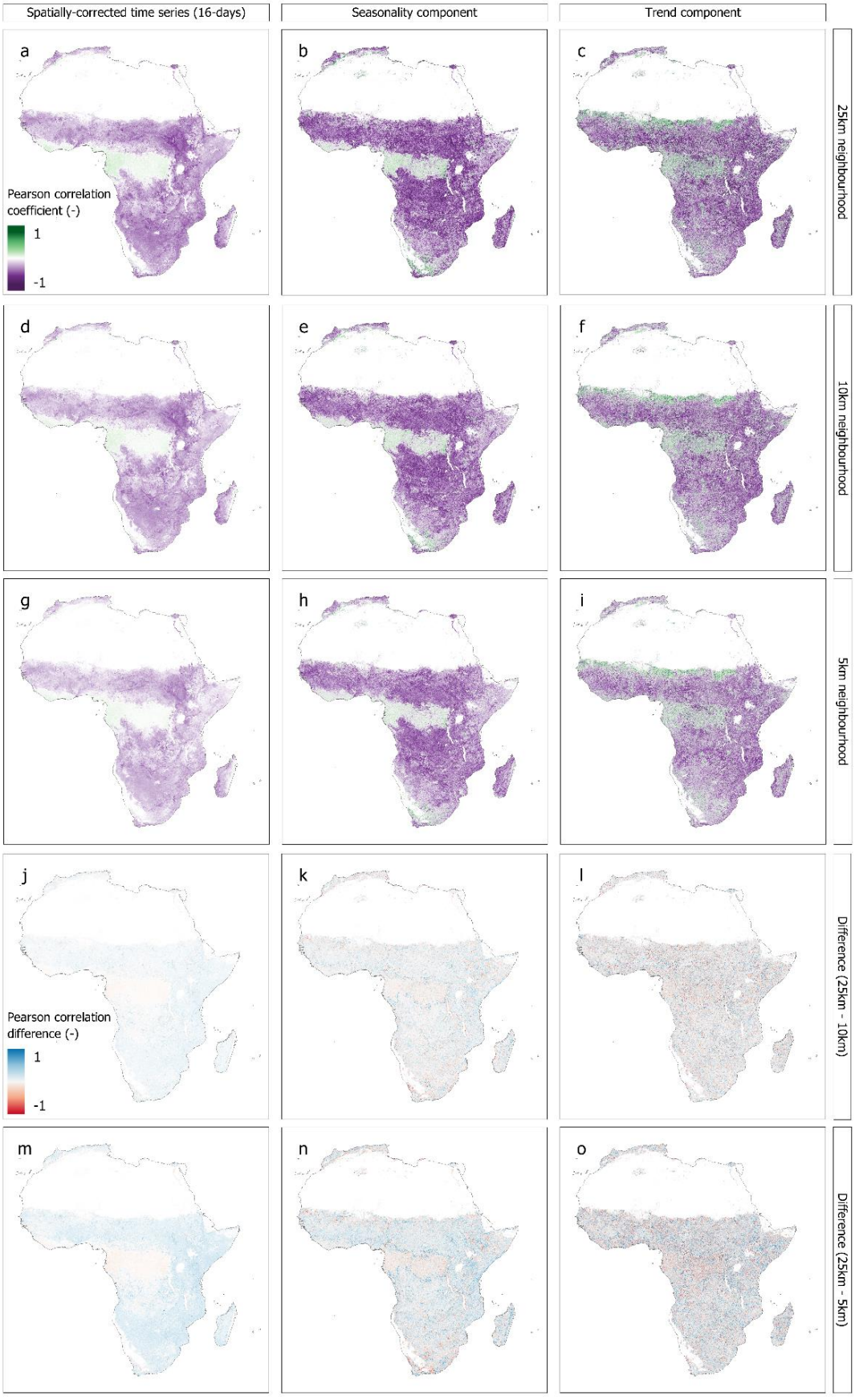

Supplementary Fig. 8 | Effect of neighbourhood radius of spatial-context method on NDVI-LST correlations. The pearson correlation coefficient between the NDVI and LST for a 25km neighbourhood (**a-c**), a 10km neighbourhood (**d-f**) and a 5km neighbourhood (**g-i**) of the 16-day, seasonal and trend components. (**j-k**) show the difference in pearson correlation coefficient between a 25km and 10km radius, (**m-o**) between a 25km and 5km radius.

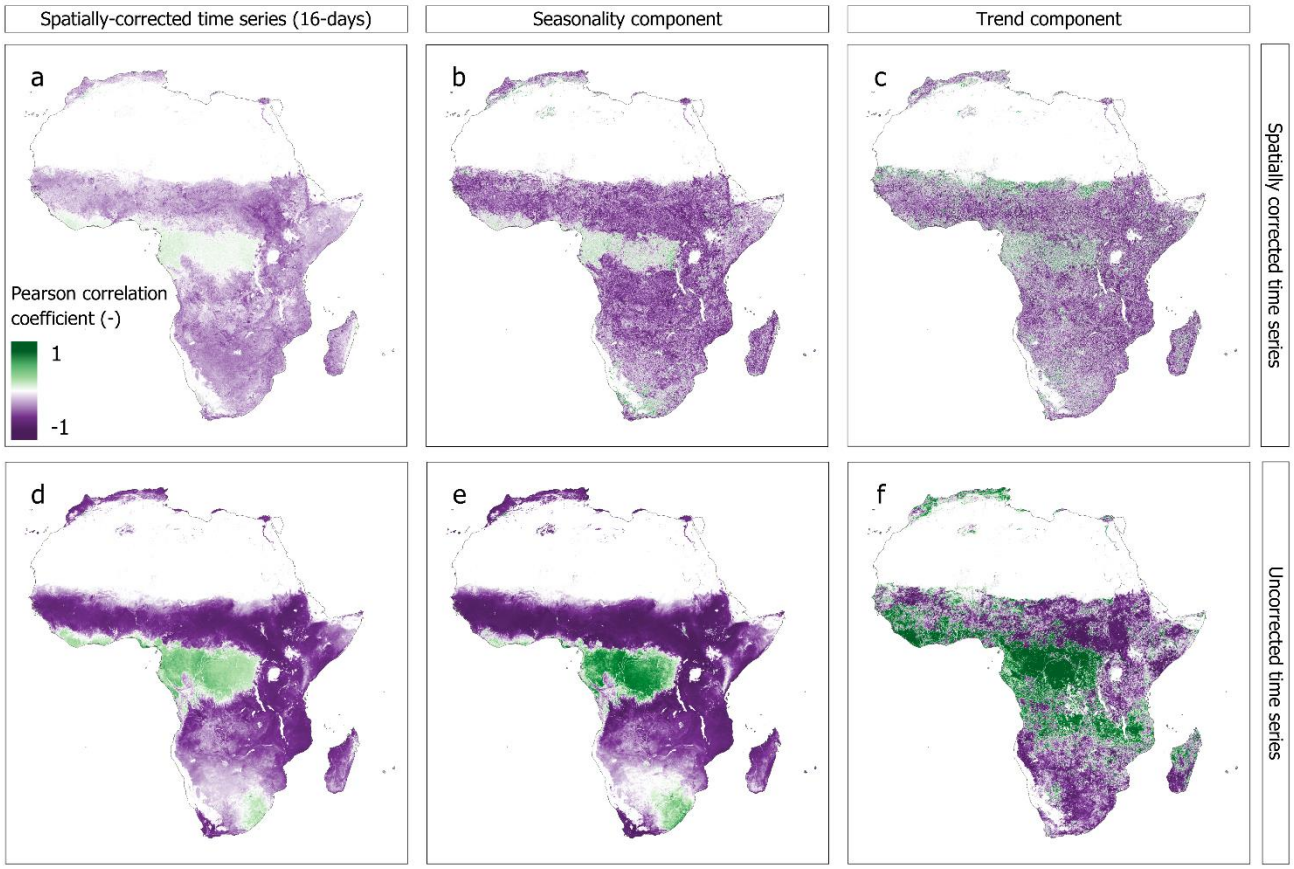

Supplementary Fig. 9 | Effect of spatial context method on NDVI-LST correlations. The pearson correlation coefficient between the NDVI and LST using the spatial context method (**a-c**) and the uncorrected time series (**d-f**) of the 16-day, seasonal and trend components.

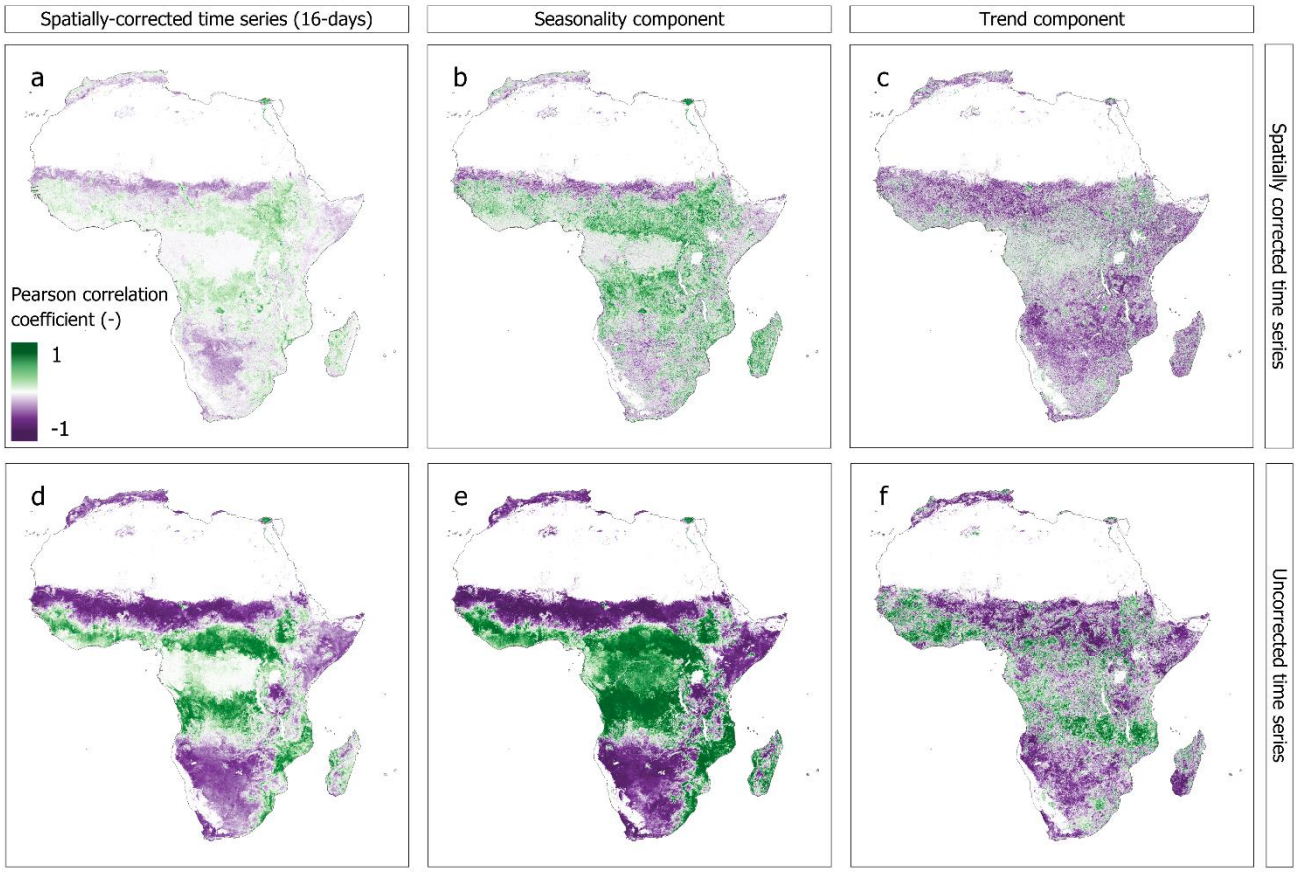

Supplementary Fig. 10 | Effect of spatial context method on NDVI-WSA correlations. The pearson correlation coefficient between the NDVI and WSA using the spatial context method (**a-c**) and the uncorrected time series (**d-f**) of the 16-day, seasonal and trend components.

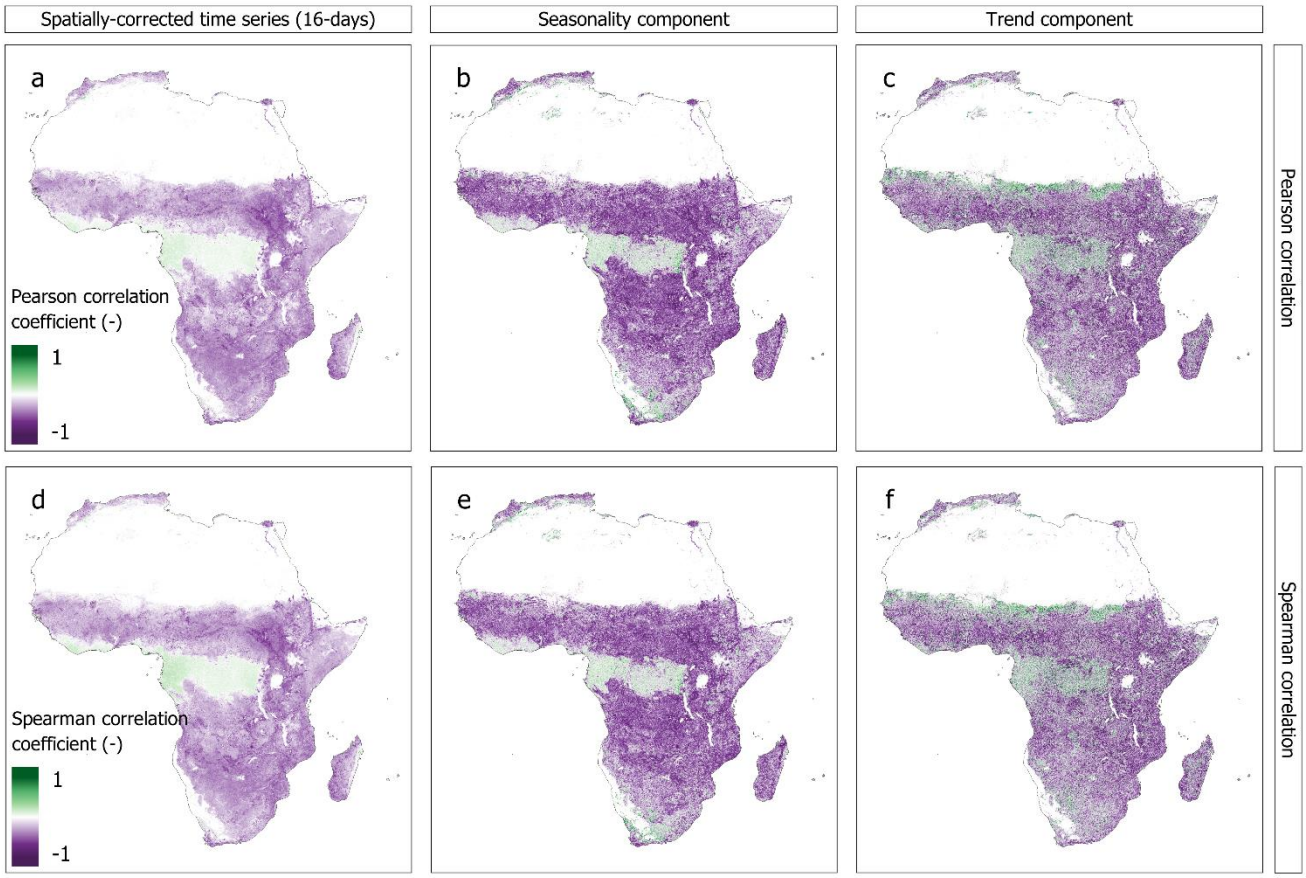

Supplementary Fig. 11 | Effect of correlation type on NDVI-LST correlations. The Pearson (**a-c**) and Spearman (**d-f**) correlation coefficient between NDVI and LST of the 16-day, seasonal and trend components.

Supplementary Table 1 | Detailed information on Eddy-covariance (EC) measurement stations.

Aridity class	Station	Country	Time period included in analysis	Source	Land use
Arid	SD-Dem	Sudan	January 2005 – December 2008	Ardö, et al. [1]	Savannas
Arid	SN-DHR	Senegal	July 2010 – December 2012	Tagesson, et al. [2]	Savannas
Semi-arid	ZA-KRU	South-Africa	January 2001 – December 2013	Archibald, et al. [3]	Savannas
Semi-arid	ZM-MON	Zambia	September 2007 – December 2008	Merbold, et al. [4]	Deciduous broadleaf forest
Humid	CG-TCH	Congo-Brazzaville	September 2006 – December 2008	Merbold, et al. [4]	Savannas
Humid	GH-ANK	Ghana	January 2011 – December 2013	Chiti, et al. [5]	Evergreen broadleaf forest

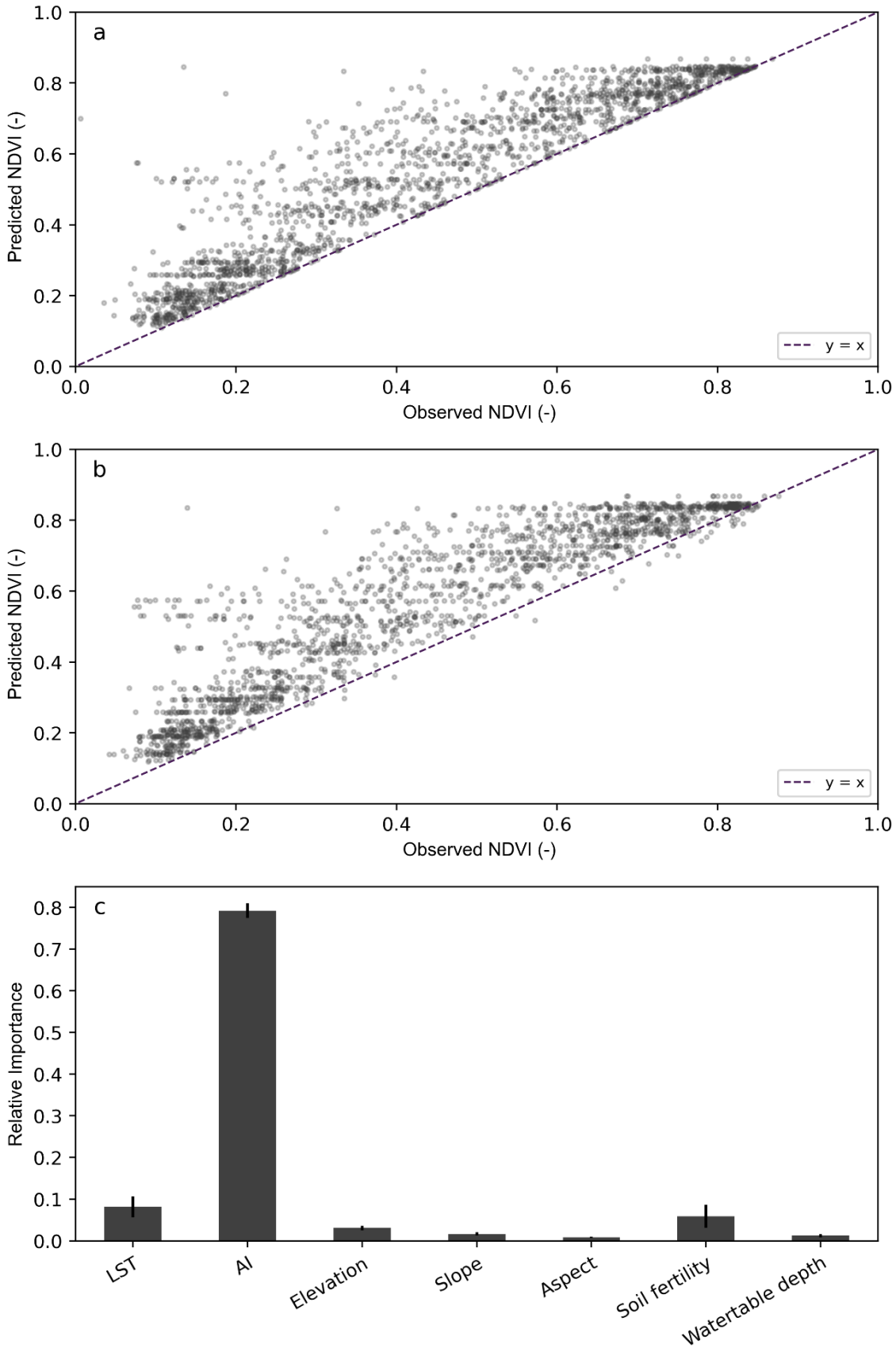

Supplementary Fig. 12 | Evaluation of potential NDVI quantile random forest regression. Observed vs prediction NDVI of training data set (**a**) and validation data set as calculated with the maximum random forest regression (**b**). Relative variable importance of maximum random forest regression, defined as the mean decrease in impurity (**c**).

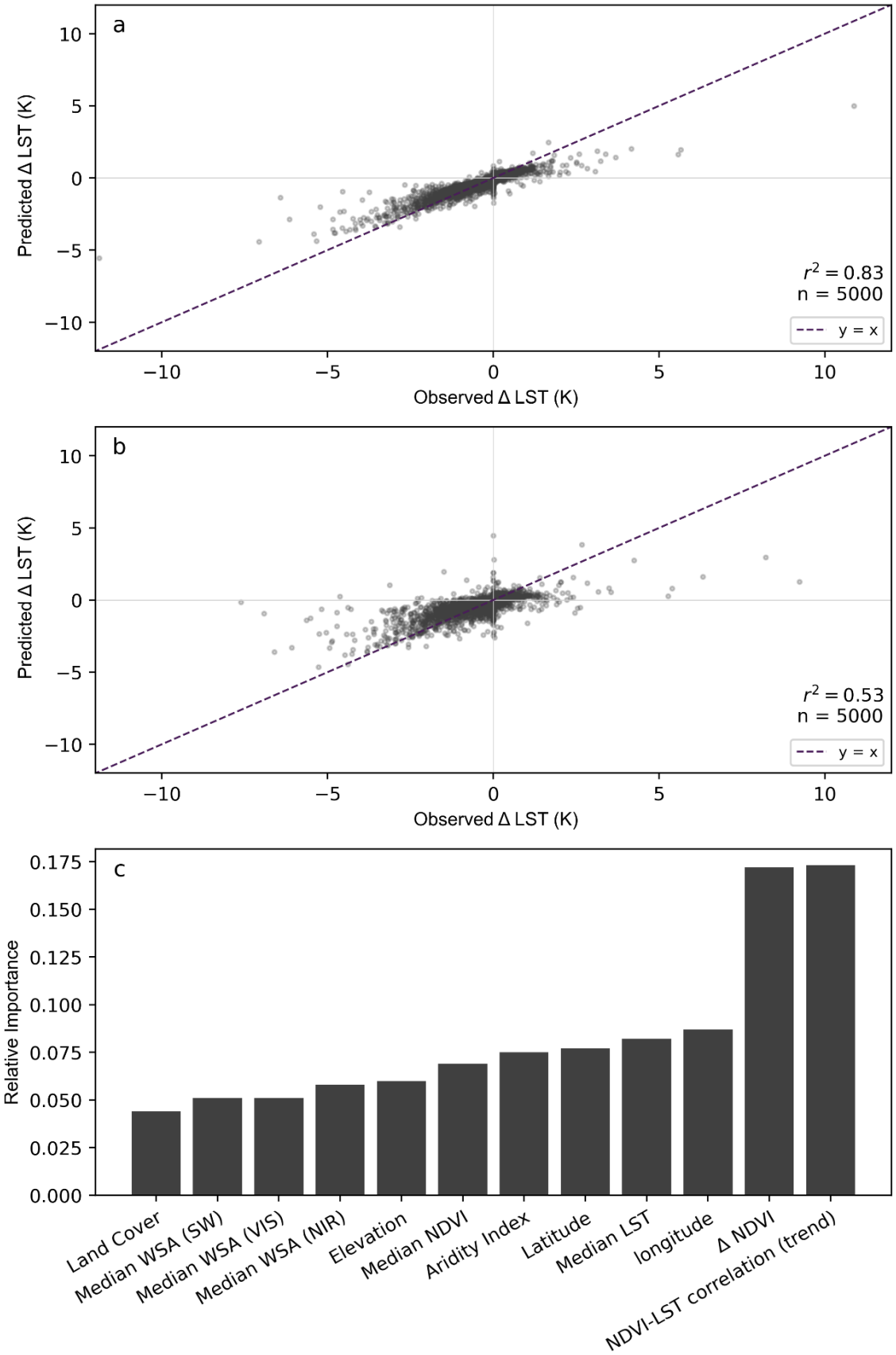

Supplementary Fig. 13 |Evaluation of ΔLST/ΔNDVI random forest regression. Observed vs prediction ΔLST/ΔNDVI of training data set (**a**) and validation data set as calculated with the random forest regression (**b**). Relative variable importance of random forest regression, defined as the mean decrease in impurity(**c**).

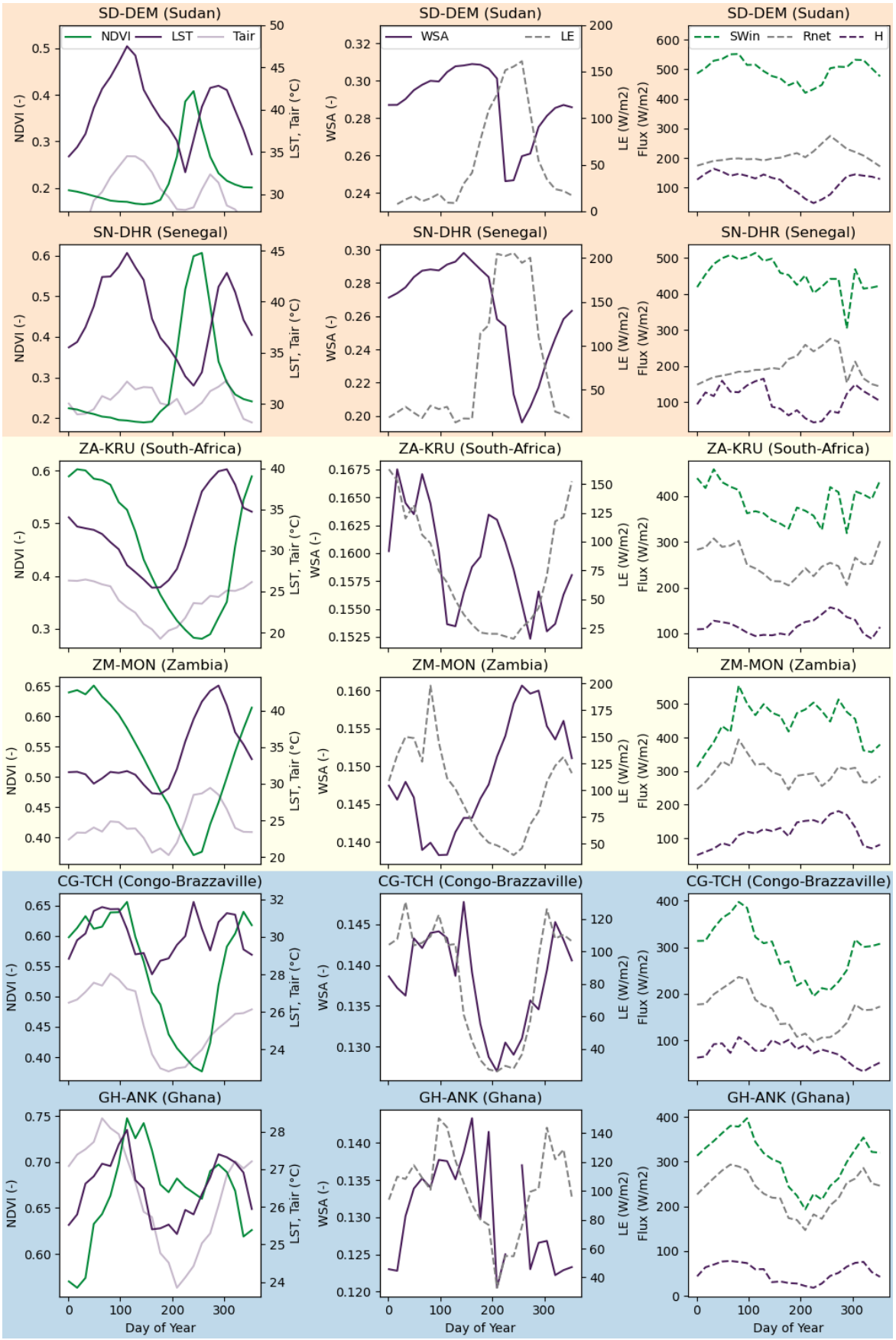

Supplementary Fig. 14| Eddy-covariance measurements at different locations in Africa. Mean uncorrected NDVI, LST, WSA, air temperature (Tair), latent heat flux (LE), sensible heat flux (H) and Net available radiation (Rnet) for each day of the year. LST is converted to °C to match Tair.

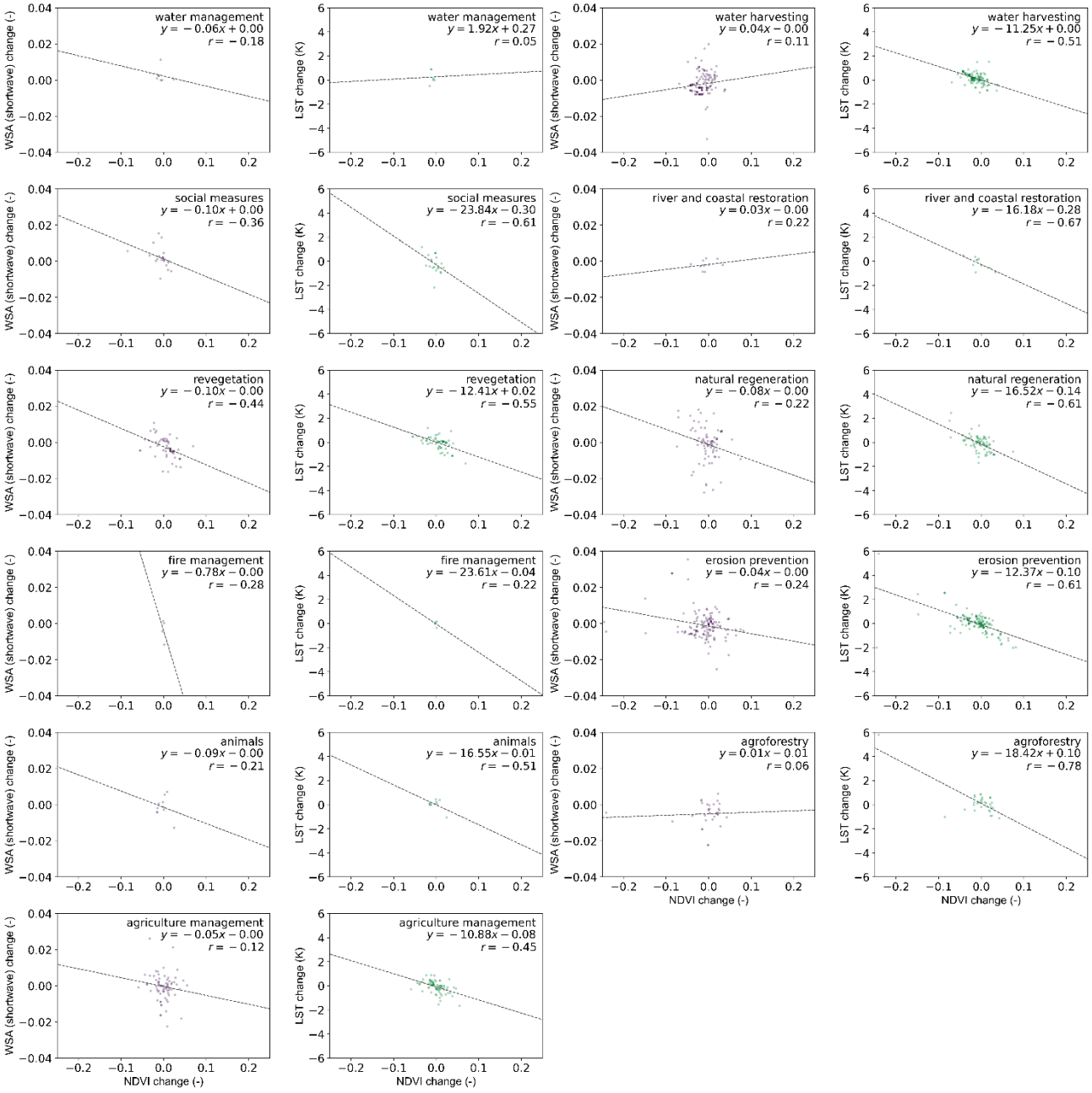

Supplementary Fig. 15 | Effect of SLM type on NDVI-WSA and NDVI-LST relations. Relation between median change in trend component of the NDVI and WSA (purple) and the NDVI and LST (green) for different types of sustainable land management projects. The projects were classified based on their provided description. Strongest NDVI-WSA correlations are found for revegetation. Strongest NDVI-LST correlations are found for agroforestry. It should be noted that not all project types have the same number of projects.

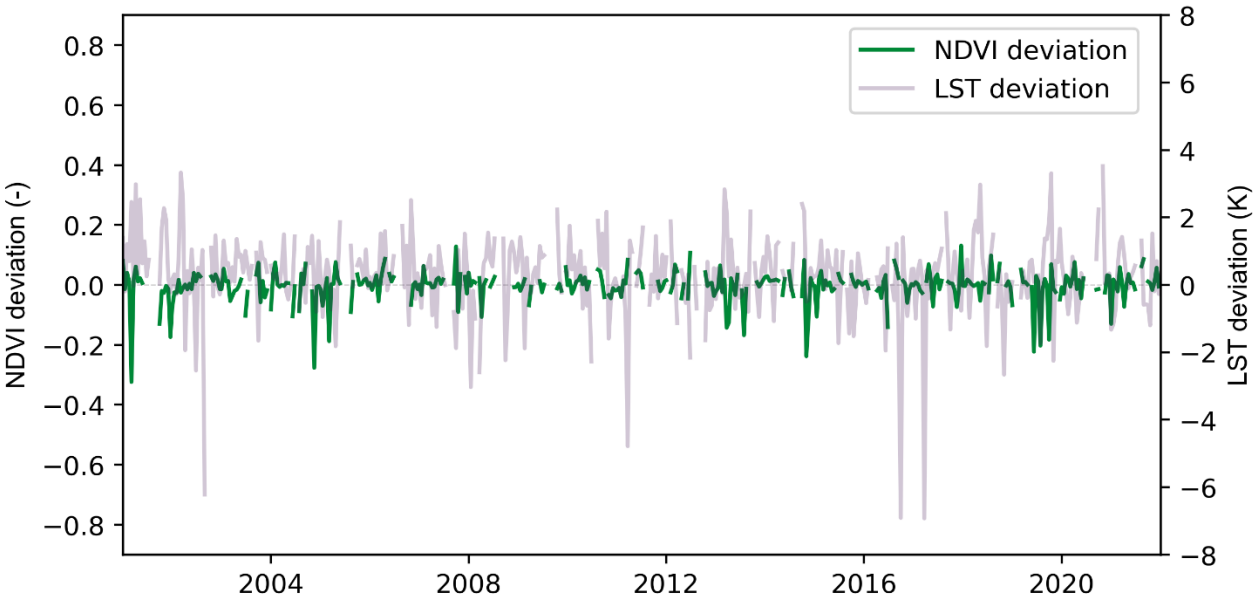

Supplementary Fig. 16 | Time series of NDVI and LST deviation. The spatially corrected NDVI and LST time series at 15.2˚E, 1.77°N (Republic of the Congo). This time series is illustrative of humid regions, were there are large amounts of noise in the time series data.

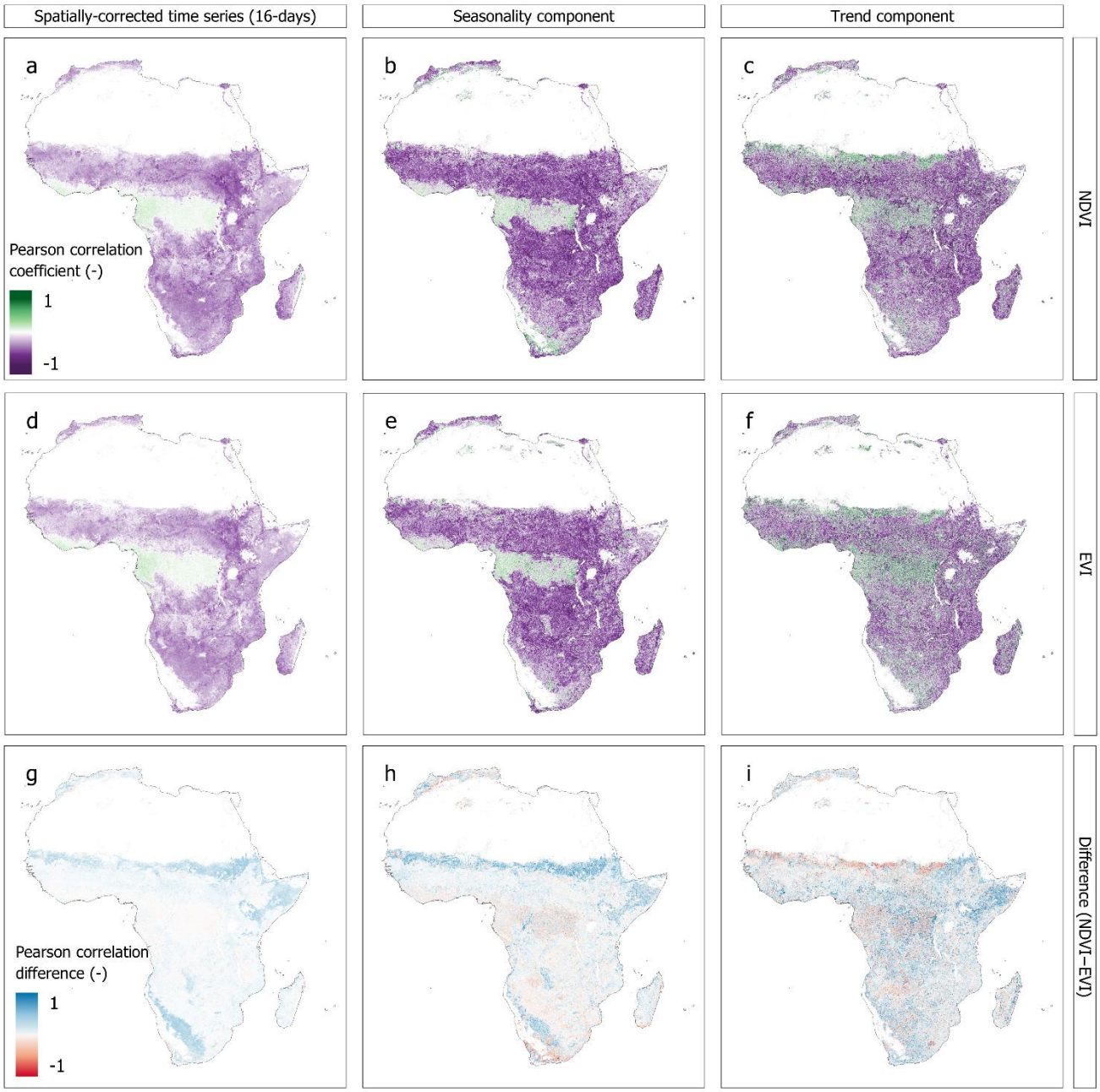

Supplementary Fig. 17 | Effect of input data on NDVI-LST and EVI-LST correlations. The pearson correlation coefficient between the NDVI and LST spatially corrected time series (**a-c**) and between the EVI and LST spatially corrected time series (**d-f**) of the 16-day, seasonal and trend components. (**g-i**) show the difference in pearson correlation coefficient between the NDVI and EVI dataset (EVI subtracted from NDVI).

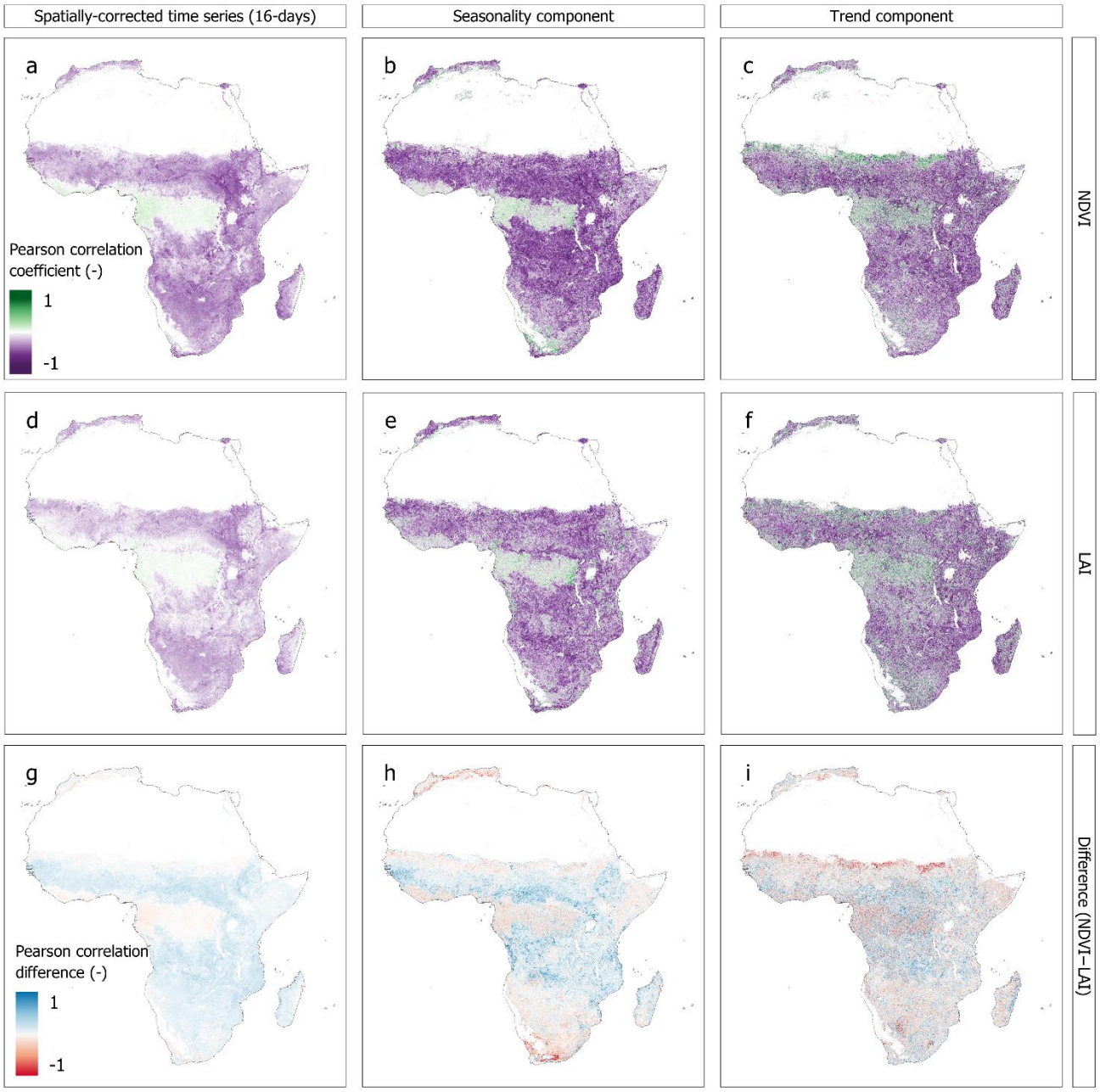

Supplementary Fig. 18 | Effect of input data on NDVI-LST and LAI-LST correlations. The pearson correlation coefficient between the NDVI and LST spatially corrected time series (**a-c**) and between the LAI and LST spatially corrected time series (**d-f**) of the 16-day, seasonal and trend components. (**g-i**) show the difference in pearson correlation coefficient between the NDVI and LAI dataset (LAI subtracted from NDVI).

Supplementary References

1 Ardö, J., Mölder, M., El-Tahir, B. A. & Elkhidir, H. A. M. Seasonal variation of carbon fluxes in a sparse savanna in semi arid Sudan. *Carbon balance and management* **3**, 1-18 (2008).

2 Tagesson, T. *et al.* Ecosystem properties of semiarid savanna grassland in West Africa and its relationship with environmental variability. *Global change biology* **21**, 250-264 (2015).

3 Archibald, S. *et al.* Drivers of inter-annual variability in Net Ecosystem Exchange in a semi-arid savanna ecosystem, South Africa. *Biogeosciences* **6**, 251-266 (2009).

4 Merbold, L. *et al.* Precipitation as driver of carbon fluxes in 11 African ecosystems. *Biogeosciences* **6**, 1027-1041 (2009).

5 Chiti, T., Certini, G., Grieco, E. & Valentini, R. The role of soil in storing carbon in tropical rainforests: the case of Ankasa Park, Ghana. *Plant and soil* **331**, 453-461 (2010).